

MICROSCOPIC CALCULATION OF TOTAL ORDINARY MUON CAPTURE RATES FOR MEDIUM - WEIGHT AND HEAVY NUCLEI

V. A. Kuz'min¹, T. V. Tetereva² K. Junker³ and A. A. Ovchinnikova²

¹ *Joint Institute for Nuclear Research, Dubna, Moscow region, 141980, Russia*

² *Skobeltsyn Institute of Nuclear Physics, Lomonosov Moscow State University,
Moscow, Russia*

³ *Paul Scherrer Institut, CH-5232 Villigen-PSI, Switzerland*

PAUL SCHERRER INSTITUT

CH - 5232 Villigen PSI

Telephon 0041 56 310 2111

Telefax 0041 56 310 2199

Microscopic Calculation of Total Ordinary Muon Capture Rates for Medium - Weight and Heavy Nuclei

V. A. Kuz'min¹, T. V. Tetereva², K. Junker³, and A. A. Ovchinnikova²

¹ *Joint Institute for Nuclear Research, Dubna, Moscow region, 141980, Russia*

² *Skobeltsyn Nuclear Physics Institute, Lomonosov Moscow State University,
Moscow, Russia*

³ *Paul Scherrer Institute, CH-5232 Villigen-PSI, Switzerland*

Abstract

Total Ordinary Muon Capture (OMC) rates are calculated on the basis of the Quasiparticle Random Phase Approximation for several spherical nuclei from ^{90}Zr to ^{208}Pb . It is shown that total OMC rates calculated with the free value of the axial-vector coupling constant g_A agree well with the experimental data for medium-size nuclei and exceed considerably the experimental rates for heavy nuclei. The sensitivity of theoretical OMC rates to the nuclear residual interactions is discussed.

1 Introduction

The main aim of investigating muon capture on atomic nuclei is the determination of the coupling constants of the weak hadronic current in the nuclear environment. In principle one is interested in the weak axial-vector g_A and pseudoscalar g_P coupling constants. The observables of nuclear muon capture are calculated as functions of g_A and g_P and then compared to the corresponding experimental data. The Radiative Muon Capture (RMC) is traditionally considered as the most promising source of information on g_P [1]. The sensitivity to g_P could be increased if one considers the ratio of the total RMC rate to the total Ordinary Muon Capture (OMC) rate [2, 3]. Therefore the problem arises how to make consistent calculations of the total RMC and OMC rates within the same nuclear model.

The investigation of total OMC rates is also of interest in itself because it allows the determination of g_A independent from beta-decay. In contrast to beta-decay all the final nuclear states with noticeable transition strength can be populated in muon capture. Therefore, small variations in the low-energy parts of theoretical strength functions give no dramatic changes in the calculated OMC rates in contrast to calculations of $\log(ft)$ values. An additional advantage of muon capture as compared to beta decay is that the total OMC rates are measured for many stable and long-living nuclei. Therefore, one can in OMC not only study the variation of g_A with nuclear mass, but more delicate effects, such as the isotopic dependence of the effective weak interaction constants between leptons and nucleons.

The present situation in the field of OMC rate measurements can be summarized as follows. Total OMC rates have been measured for many nuclei with high precision [4]. The theoretical interpretation of the experimental information is, however, still controversial. The main reason lies in the necessity of a correct description of the nuclear response in both, OMC and RMC.

The theoretical investigation of nuclear muon capture has a rather long history. Up to now, three different approaches have been developed for calculating total (exclusive) OMC rates on complex nuclei. The first approach is based on the closure approximation and related sum rule methods. In both cases the energy of the outgoing neutrino is replaced by some average value which is a parameter of the theory. The OMC rate is then obtained using the closure relation for the final nuclear states [5, 6]. The second approach utilizes the local density approximation. Here the OMC rates are calculated for infinite and uniform nuclear matter as a function of the proton and neutron densities. The OMC rate for a finite-size nucleus is then obtained by integrating this function over the realistic density distribution or by determining its value for a certain value of the nuclear matter density [7, 8]. The common drawback of

both approaches is that nuclear muon capture is considered without any connection to other processes which may occur in a nucleus. Also, the collective nature of the nuclear response to external fields is lost. The third approach, which is used in this paper, does not suffer from these defects. Here the (exclusive) OMC rates are calculated for all definite final states of the product nucleus and the total rate is obtained by summing over all considered final states.

$$\Lambda_{\text{tot}} = \sum_f \Lambda_{fi}. \quad (1)$$

The calculations of Refs. [3, 9, 10, 11, 12] have been carried out within this approach.

In the present work we study the total OMC rates on heavy nuclei within a microscopic description of the nuclear structure. The one-body effective Hamiltonian of nuclear OMC obtained within the Morita and Fujii formalism [13] is used. The wave function of the bound muon and its binding energy are calculated approximately [14], taking into account the finite size of the nucleus. The nuclear matrix elements of the effective OMC Hamiltonian and the excitation energies of the states of a product nucleus are calculated within the Quasiparticle Random Phase Approximation (QRPA), an extension of the usual RPA to nonclosed shell nuclei. Velocity-dependent terms are included in the calculations and have been evaluated with Woods-Saxon single-particle wave functions having the correct asymptotic behaviour.

2 The Effective Hamiltonian of Nuclear Muon Capture

The total rate of OMC is calculated by summing the rates Λ_{fi} for all partial transitions $i \rightarrow f$. In a spherically symmetric nucleus Λ_{fi} is given by [15]

$$\Lambda_{fi} = [G \cos \Theta_C]^2 (E_\nu)^2 \left(1 - \frac{E_\nu}{M_i + m_\mu}\right) \frac{2J_f + 1}{2J_i + 1} \sum_u (M_u^2(u) + M_u^2(u+1) + M_u^2(-u) + M_u^2(-u-1)) \quad (2)$$

The $M_u(\kappa)$'s are the amplitudes for the transition in which a neutrino is created in a state with energy E_ν and angular quantum number κ ($\kappa = l$ for $j = l - 1/2$ and $\kappa = -l - 1$ for $j = l + 1/2$). u is the angular momentum transferred to the nucleus. These amplitudes are combinations of the weak form factors with nuclear matrix elements

$$\begin{aligned}
M_u(u) &= \sqrt{\frac{2}{2u+1}} \left(\sqrt{u} G_V [0uu] - \sqrt{\frac{u+1}{3}} G_A [1uu] \right. \\
&\quad \left. - \sqrt{\frac{2u+1}{3}} \frac{g_V}{M} [1u-1up] \right) \\
M_u(-u-1) &= \sqrt{\frac{2}{2u+1}} \left(\sqrt{u+1} G_V [0uu] + \sqrt{\frac{u}{3}} G_A [1uu] \right. \\
&\quad \left. - \sqrt{\frac{2u+1}{3}} \frac{g_V}{M} [1u+1up] \right) \\
M_u(-u) &= \sqrt{\frac{2}{2u+1}} \left(-\sqrt{\frac{2u+1}{3}} (G_A - \frac{u}{2u+1} G_P) [1u-1u] \right. \\
&\quad + \sqrt{\frac{u(u+1)}{3(2u+1)}} G_P [1u+1u] - \sqrt{u} \frac{g_A}{M} [0uup] \\
&\quad \left. + \sqrt{\frac{u+1}{3}} \frac{g_V}{M} [1uup] \right) \\
M_u(u+1) &= \sqrt{\frac{2}{2u+1}} \left(-\sqrt{\frac{u(u+1)}{3(2u+1)}} G_P [1u-1u] + \sqrt{\frac{2u+1}{3}} (G_A \right. \\
&\quad \left. - \frac{u+1}{2u+1} G_P) [1u+1u] + \sqrt{u+1} \frac{g_A}{M} [0uup] + \sqrt{\frac{u}{3}} \frac{g_V}{M} [1uup] \right)
\end{aligned} \tag{3}$$

Here the effective form factors are defined in the usual way

$$\begin{aligned}
G_V &= g_V(q^2)(1 + E_\nu/2M) + g_S(q^2) \\
G_A &= g_A(q^2) - (g_V(q^2) + g_M(q^2))(E_\nu/2M) \\
G_P &= (g_P(q^2) - g_A(q^2) - g_T(q^2) - g_V(q^2) - g_M(q^2))(E_\nu/2M)
\end{aligned} \tag{4}$$

and the nuclear single-particle matrix elements are given by

$$\begin{aligned}
[0uu] &= \langle J_f \parallel \sqrt{\frac{1}{4\pi}} \sum_{k=1}^A \phi_\mu(r_k) t_k^+ j_u(E_\nu r_k) Y_u(\hat{r}_k) \parallel J_i \rangle / \sqrt{2J_f + 1} \\
[1wu] &= \langle J_f \parallel \sqrt{\frac{3}{4\pi}} \sum_{k=1}^A \phi_\mu(r_k) t_k^+ j_w(E_\nu r_k) [\sigma \otimes Y_w(\hat{r}_k)]_u \parallel J_i \rangle / \sqrt{2J_f + 1} \\
[1wup] &= i \langle J_f \parallel \sqrt{\frac{3}{4\pi}} \sum_{k=1}^A \phi_\mu(r_k) t_k^+ j_w(E_\nu r_k) [Y_w(\hat{r}_k) \otimes p_k]_u \parallel J_i \rangle / \sqrt{2J_f + 1} \\
[0uup] &= i \langle J_f \parallel \sqrt{\frac{1}{4\pi}} \sum_{k=1}^A \phi_\mu(r_k) t_k^+ j_u(E_\nu r_k) Y_u(\hat{r}_k) (\vec{p}_k, \vec{\sigma}_k) \parallel J_i \rangle / \sqrt{2J_f + 1}
\end{aligned} \tag{5}$$

where $j_u(x) = \sqrt{\pi/2x} J_{u+1/2}(x)$ is a spherical Bessel function and

$$[\sigma \otimes Y_w(\hat{r})]_{u,m_u} = \sum_{m,m_w} \langle 1m w m_w | u m_u \rangle \sigma_m Y_{w,m_w}(\hat{r}) \tag{6}$$

is the tensor product of two spherical tensor operators. $\phi_\mu(r)$ is the radial wave function of the bound muon. For the nucleon isospin operators t^+ the convention $t^+|p\rangle = |n\rangle$ is used.

Eqs.(2) and (5) show that the capture rate depends rather strongly on the energy of the outgoing neutrino

$$E_\nu = (m_\mu - |\epsilon_{1S}| + M_i - M_f - E^*)(1 - \frac{m_\mu - |\epsilon_{1S}| + M_i - M_f - E^*}{2(m_\mu + M_i)}) \quad (7)$$

For a large Z nucleus the muon binding energy ϵ_{1S} has to be calculated taking into account the finite size of the nuclear charge distribution. The excitation energy of the final nuclear state E^* enters into the capture rate mainly through the neutrino energy. In order to obtain the transition energies and nuclear matrix elements (5) one has to use some nuclear model. In the present work the QRPA has been used since it gives a precise prescription of how the interaction between particle and hole excitation can be included in the calculation of the nuclear matrix elements (5) and the excitation spectrum of the product nucleus.

3 The Nuclear Model

A detailed description of the nuclear model used in the present work can be found in [3] and will not be repeated here. The nuclear Hamiltonian consists of a mean field part, a monopole pairing interaction between like particles and a residual interaction.

$$H_M = \sum_{t_3=\pm 1/2} \left(H_{\text{mean}}(t_3) + H_{\text{pair}}(t_3) \right) + H_{\text{resid}} \quad (8)$$

For protons and neutrons separate Woods-Saxon potentials including spin-orbit interactions have been used to approximate the mean field. The mean field and pairing Hamiltonians

$$\begin{aligned} H_0(t_3) &= H_{\text{mean}}(t_3) + H_{\text{pair}}(t_3) \\ &= \sum_{j,m} E_{jt_3} a_{jmt_3}^\dagger a_{jmt_3} - \frac{G_{t_3}}{4} \sum_{jm,j'm'} (-1)^{j-m+j'-m'} a_{jmt_3}^\dagger a_{j,-mt_3}^\dagger a_{j',-m't_3} a_{j',m't_3} \end{aligned} \quad (9)$$

are in a first step approximately diagonalized by the special Bogoliubov transformation (see e.g. [16])

$$a_{jmt_3} = u_{jt_3} \alpha_{jmt_3} + (-1)^{j-m} v_{jt_3} \alpha_{j,-mt_3}^\dagger. \quad (10)$$

Solving the BCS equations leads to the Independent Quasiparticle Hamiltonian

$$H_0(t_3) \rightarrow \sum_{jm} \epsilon_{jt_3} \alpha_{jmt_3}^\dagger \alpha_{jmt_3} \quad (11)$$

with

$$\epsilon_{jt_3} = \sqrt{(E_{jt_3} - \lambda_{t_3})^2 + C_{t_3}^2} \quad \text{and} \quad C_{t_3} = \frac{G_{t_3}}{2} \sum_{j,m} u_{jt_3} v_{jt_3}. \quad (12)$$

An averaging over the quasiparticle vacuum state $\alpha_{jmt_3}|0\rangle = 0$ is implied. As residual interaction we use an effective isospin-invariant separable interaction of the form

$$H_{\text{resid}} = -\frac{1}{2} \sum_{L,M} (\kappa_0^L + \kappa_1^L (\vec{\tau}_1 \cdot \vec{\tau}_2)) Q_{LM}^\dagger(1) Q_{LM}(2) - \frac{1}{2} \sum_{L,J,M} (\kappa_0^{LJ} + \kappa_1^{LJ} (\vec{\tau}_1 \cdot \vec{\tau}_2)) Q_{LJM}^\dagger(1) Q_{LJM}(2). \quad (13)$$

where Q_{LM} and Q_{LJM} are single-particle multipole and spin-multipole operators and the isospin structure is displayed explicitly. Using

$$(\vec{\tau}_1 \cdot \vec{\tau}_2) = 4(\vec{t}_1 \cdot \vec{t}_2) = 4t_1^0 t_2^0 + 2(t_1^- t_2^+ + t_1^+ t_2^-). \quad (14)$$

one can combine the isospin operators with the multipole and spin-multipole operators leading to a new set of single-particle operators

$$Q_{LM}^\rho(k) = \sum_{j'm't'_3, jmt_3} \langle j'm't'_3 | i^L f_L(r_k) Y_{LM}(k) t_k^\rho | jmt_3 \rangle a_{j'm't'_3}^\dagger a_{jmt_3} \quad (15)$$

and

$$Q_{LJM}^\rho(k) = \sum_{j'm't'_3, jmt_3} \langle j'm't'_3 | i^L f_{LJ}(r_k) [Y_L(k) \otimes \sigma(k)]_{JM} t_k^\rho | jmt_3 \rangle a_{j'm't'_3}^\dagger a_{jmt_3} \quad (16)$$

where t_k^ρ is an isospin operator out of the set $\{\hat{1}_k, t_k^0 = t_k^z, t_k^\pm = t_k^x \pm it_k^y, (k = 1, 2)\}$. In the literature [18] one finds two most frequently used variants of the radial form factors $f_L(r)$ and $f_{LJ}(r)$. These are

$$f_L(r) = f(r)_{LJ} = r^L. \quad (17)$$

and

$$f_L(r) = f(r)_{LJ} = f(r) = \frac{d}{dr} U(r), \quad (18)$$

where $U(r)$ is the central part of the shell-model potential used in H_{mean} . The mixed products $t_1^- t_2^+$ and $t_1^+ t_2^-$ in Eq.(14) lead to particle-hole excitations changing the charge of the nucleus and are therefore involved in a description of charge-exchange interaction processes such as β -decay, μ -capture or direct (p, n) and (n, p) reactions. The corresponding parts in the Hamiltonian (13) are constructed with the single-particle operators

$$\Omega_{JM} = \sum_{j_n m_n, j_p m_p} \langle j_n m_n | O_{JM} t^+ | j_p m_p \rangle a_{j_n, m_n}^\dagger a_{j_p, m_p} \quad (19)$$

and their Hermitian conjugates, where O_{JM} can be either $i^J f_J(r) Y_{JM}(\hat{r})$ or $i^L f_{LJ}(r) [Y_L(\hat{r}) \otimes \sigma]_{JM}$ respectively.

The residual interaction (13) contains only scalar products of the form $([Y_{J-1}(\hat{r}_1) \otimes \sigma_1]_J, [Y_{J-1}(\hat{r}_2) \otimes \sigma_2]_J)$ and $([Y_{J+1}(\hat{r}_1) \otimes \sigma_1]_J, [Y_{J+1}(\hat{r}_2) \otimes \sigma_2]_J)$. The

tensor interaction which would mix the $[Y_{J-1}(\hat{r}_1) \otimes \sigma_1]_{JM}$ and $[Y_{J+1}(\hat{r}_2) \otimes \sigma_2]_{JM}$ terms has been omitted because its inclusion would slightly influence the properties of the charge-exchange resonances in the range where the coupling constants assume reasonable values.

To achieve an approximate diagonalization of the residual interaction Hamiltonian in the QRPA one introduces phonon creation and destruction operators. They are defined as linear combinations of tensor products of the quasiparticle operators α_{jmt_3} and $\alpha_{j'm't'_3}$ and their Hermitian conjugates (Eq.10).

$$\Omega_{JM}^i = \sum_{j_p, j_n} \left(\psi_{j_p, j_n}^i [\alpha_{j_p} \otimes \alpha_{j_n}]_{J,M} - (-1)^{J-M} \phi_{j_p, j_n}^i [\alpha_{j_p} \otimes \alpha_{j_n}]_{J,-M}^\dagger \right) \quad (20)$$

The phonon amplitudes ψ_{j_n, j_p}^i and ϕ_{j_n, j_p}^i are orthonormalized according to

$$\Phi(i, i') \equiv \sum_{j_p, j_n} \{ \psi_{j_p, j_n}^i \psi_{j_p, j_n}^{i'} - \phi_{j_p, j_n}^i \phi_{j_p, j_n}^{i'} \} = \delta_{i, i'}. \quad (21)$$

Having expressed the residual interaction in terms of the phonon operators (20) one obtains the QRPA equations through a variational principle [16]

$$\delta \left\{ \langle |\Omega_{JM}^i H_M \Omega_{JM}^i{}^\dagger| \rangle - \langle |H_M| \rangle - \omega_i (\Phi(i, i) - 1) \right\} = 0 \quad (22)$$

using the normalization of the phonon amplitudes as a subsidiary condition. $|\rangle$ is the phonon vacuum: $\Omega_{JM}^i |\rangle = 0$, approximating the ground state of a double even nucleus. The QRPA equations resulting from (22) are a system of homogeneous linear equations determining the phonon amplitudes ψ_{j_n, j_p}^i and ϕ_{j_n, j_p}^i and the excitation energies ω_i .

$$\begin{aligned} R_{q, q'}^+ g_{q'}^i - \omega_i w_q^i &= 0, \\ -\omega_i g_q^i + R_{q, q'}^- w_{q'}^i &= 0, \end{aligned} \quad (23)$$

where the following abbreviations have been used

$$g_q^i = \psi_{j_p, j_n}^i + \phi_{j_p, j_n}^i, \quad w_q^i = \psi_{j_p, j_n}^i - \phi_{j_p, j_n}^i, \quad q \equiv (j_p, j_n), \quad (24)$$

$$\epsilon_q = \epsilon_{j_p} + \epsilon_{j_n}, \quad u_q^\pm = u_{j_p} v_{j_n} \pm v_{j_p} u_{j_n} \quad (25)$$

$$R_{q, q'}^\pm = \epsilon_q \delta_{q, q'} - \frac{2}{2J+1} \left(\kappa_1^J h_q^J u_q^\pm h_{q'}^J u_{q'}^\pm + \kappa_1^{JJ} h_q^{JJ} u_q^\pm h_{q'}^{JJ} u_{q'}^\pm \right) \quad (26)$$

for naturally parity states and

$$R_{q, q'}^\pm = \epsilon_q \delta_{q, q'} - \frac{2}{2J+1} \left(\kappa_1^{J-1, J} h_q^{J-1, J} u_q^\pm h_{q'}^{J-1, J} u_{q'}^\pm + \kappa_1^{J+1, J} h_q^{J+1, J} u_q^\pm h_{q'}^{J+1, J} u_{q'}^\pm \right) \quad (27)$$

for unnatural parity states. h_q^J and h_q^{LJ} stand for the reduced matrix elements of the multipole (15) and spin-multipole (16) single-particle operators with $t^p = t^-$. The

QRPA amplitudes for the transitions from the even-even ground state to the excited states with total spin JM , and energies $\omega_i \pm (\lambda_n - \lambda_p)$ are given by

$$b_{JM}^+(i) = \frac{1}{\sqrt{2J+1}} \sum_{j_p, j_n} \langle j_p \| O_{Jt^-} \| j_n \rangle (v_{j_p} u_{j_n} \psi_{j_p, j_n}^i + u_{j_p} v_{j_n} \phi_{j_p, j_n}^i) \quad (28)$$

if the charge of the nucleus decreases from Z to $Z - 1$ (as, for example, in (n, p) reactions) or by

$$b_{JM}^-(i) = \frac{1}{\sqrt{2J+1}} \sum_{j_p, j_n} \langle j_p \| O_{Jt^-} \| j_n \rangle (u_{j_p} v_{j_n} \psi_{j_p, j_n}^i + v_{j_p} u_{j_n} \phi_{j_p, j_n}^i) \quad (29)$$

if the charge increases from Z to $Z + 1$ during the transition (as in (p, n) reactions).

In the following we will make a few remarks on the nuclear model parameters. There are three kinds of parameters which characterize the nuclear structure of our model Hamiltonian. The parameters of the mean field (Woods-Saxon potential) are determined such that they reproduce best the single-particle excitations of neighbouring odd-mass nuclei. Different potentials have been used for protons and neutrons. The parameters of the monopole pairing interaction have been obtained from the odd-even effect of nuclear binding energies. Since the theoretical binding energies depend on the single-particle energies there is a certain correlation between the pairing constants and the parameters of the Woods-Saxon potential. Usually one set of monopole pairing constants and Woods-Saxon potential parameters has been used in the calculations for a whole group of neighbouring nuclei. These parameter sets have been taken from [17]. The residual interaction between particle-hole excitations causes the collective small amplitude vibrations. The effective constants of this interaction have been determined by comparing the calculated excitation energies and the transition strengths of the collective isovector states with experiment. In the present work only the isovector interaction is of interest since we are dealing with a charge changing process. A detailed discussion of the used form of separable residual interaction can be found in the work of [18]. In order to demonstrate the sensitivity of the calculated total muon capture rate Λ_{tot} to the residual interaction, both variants of radial form factors have been used with several values for the isovector coupling constant.

4 Results of the Calculations

In this section we present detailed results of the calculated total OMC rates obtained for spherical nuclei of different mass regions. The data are presented in Table 1 to Table 10. The capture rates shown in Fig. 1 and Fig. 3 are presented in the form of running sums

$$\Lambda(E) = \sum_{k: E_k < E} \Lambda_k, \quad (30)$$

where the energies are measured with respect to the ground state of the initial nucleus. In order to get a feeling for the sensitivity of the theoretical muon capture rates on the chosen shape and strength of the residual interaction, all calculations have been performed for both types of interaction (17) and (18). Throughout we have employed $g_P/g_A = 6.0$ in the calculations.

4.1 ^{90}Zr and ^{92}Mo

The distribution of the strength of the transition operator σt^- over the excitation energies (Gamow-Teller strength function) has been studied in detail for the reactions $^{90}\text{Zr}(p, n)^{90}\text{Nb}$ [19, 20] and $^{90}\text{Zr}(^6\text{Li}, ^6\text{He})^{90}\text{Nb}$ [21]. The strength function has a prominent peak at an energy of 15.6 MeV. For this peak the reduced probability of the GT transition $B(GT) = 10$. The total observed transition strength below 20 MeV excitation energy is around 20. The total GT strength should be larger than $3(N - Z) = 30$, the value given by the Ikeda sum rule [22].

Table 1 shows how the calculated properties of the GT strength function depend on κ_1^{01} and κ_1^{21} . The model of non-interacting quasiparticles (residual interaction switched off: $\kappa_1^{01} = \kappa_1^{21} = 0$) cannot give the correct position of the peak of the strength function. For $L = 0$ and $J = 1$, the residual interaction (17) reduces to the simple $(\vec{\sigma}, \vec{\sigma})$ interaction considered in [23]. The calculations with $\kappa_1^{01} = -23/A$ recommended in [23] correctly reproduce the position of the maximum of the strength function. The results of calculations with slightly different constants $\kappa_1^{01} = -25/A$ and $\kappa_1^{01} = -28/A$, presented in Table 1, show that the position of the maximum of the strength function is sensitive to κ_1^{01} . The strength in the peak region does not depend on κ_1^{01} and considerably exceeds the experimentally observed one. So, the best value of the effective constant for the residual interaction (17) is $\kappa_1^{01} = -23/A$.

Table 1 shows that the calculated energy of the GT resonance is less sensitive to κ_1^{01} for the residual interaction with form factor (18). The correct position of the resonance is reproduced with $\kappa_1^{01} = -0.33/A$. Simultaneously the strength below and in the resonance region is considerably smaller than the corresponding strength calculated with interaction (17) (24.6 to be compared to 29.2) and is closer to the

experimental value. The rest of the transition strength is located at high-excited 1^+ states [24]. Recently, new experimental data of the GT transition strength at very high excitation energies became available [20]. The total $B(GT)$ strength calculated with the residual interaction (18) is equal to 32.0. This agrees with the experimental value 34.2 ± 1.6 obtained in [20] by a multipole decomposition of the experimental $^{90}\text{Zr}(p, n)^{90}\text{Nb}$ cross sections. From this consideration one concludes that the residual interaction (18) provides a better description of the σt^- strength function than the interaction (17).

Recent measurements of the σt^+ transition strength in $^{90}\text{Zr}(n, p)^{90}\text{Y}$ [25] can also be compared with our calculations, since in this reaction the charge of the nucleus decreases as in muon capture. The σt^+ strength, summed over all experimentally observed states is $B_{\Sigma}^+(GT) = 1.0 \pm 0.3$ [25]. Our calculation with the interaction (17) gives the following distribution of the transition strength. A considerable part of $B_{\Sigma}^+(GT)$ is concentrated on the first 1^+ state of ^{90}Y . The other 1^+ states have excitation energies between 10 and 15 MeV. For each of these states, $B^+(GT) < 0.2$.

The σt^+ strength function calculated with the interaction (18) differs from the strength function obtained with interaction (17). The $B_{\Sigma}^+(GT)$ calculated with interaction (18) is almost three times the value of $B_{\Sigma}^+(GT)$ obtained with interaction (17). This is due to highly excited states which are absent in the calculations with the $f(r) = r^L$ interaction. As before, the strongest transition goes to the first 1^+ state of ^{90}Y , but the strengths of transitions going to 1^+ states with energies between 5 and 15 MeV are comparable to $B_1^+(GT)$. In this case the transition strength is distributed more uniformly over the excitation energies and the shape of the theoretical strength function is closer to the experimental one.

It should be noted that the energy of the first 1^+ state calculated for each of the two residual interactions does not depend on κ_1^{01} , and the corresponding $B_1^+(GT)$ decreases slightly with growing $|\kappa_1^{01}|$. This indicates that already in ^{90}Zr the neutron excess prevents the creation of low-lying collective 1^+ states in ^{90}Y . The residual interaction with $f(r) = dU/dr$ (18) couples single-particle states with wave functions having the same orbital quantum numbers and different number of nodes in the radial parts. Due to the residual interaction (18), these particle-hole excitations interact with particle-hole states which are all members of one spin-orbital multiplet and create in this way high-excited collective states [24]. The transitions to those states increase $B_{\Sigma}^+(GT)$.

It was shown in [3] that the theoretical OMC rates are rather insensitive to the constants of the multipole residual interaction κ_1^J . Nevertheless, the constant of the isovector monopole residual interaction, κ_1^0 , can be determined from analyzing isobar analog states (IAS). Results for the 0^+ charge-exchange excitation in ^{90}Zr are presented in Table 2. The independent quasiparticle model describes the 0^+ charge-exchange

states as a set of non-interacting two-quasiparticles states. The states carrying the main transition strength are $(0g_{9/2})_p(0g_{9/2})_n$ and $(1d_{1/2})_p(1d_{1/2})_n$ for the t^- or (p, n) branch and $(0f_{7/2})_p(0f_{7/2})_n$ and $(0d_{5/2})_p(1d_{5/2})_n$ for the t^+ or (n, p) transitions. Both interactions produce a collective state in the (p, n) excitation branch whose energy coincides with the experimental IAS energy of 12.0 MeV [26] ($\kappa_1^0 = -0.43/A$ for interaction (18) and $\kappa_1^0 = -35.0/A$ for interaction (17)). In both cases this state consumes almost all of the t^- transition strength.

In the (n, p) branch the interaction (17) with the above mentioned coupling constant is not capable to produce a collective state and the strength goes into the $(0f_{7/2})_p(0f_{7/2})_n$ and $(0d_{5/2})_p(1d_{5/2})_n$ two-quasiparticle states. The interaction (18) with the above mentioned coupling constant is strong enough to produce a collective state at approximately the energy of the two-quasiparticle states. The difference between the total t^- and t^+ transition strengths is constant and does not depend on the residual interaction. Therefore one can use the strength functions to determine the isovector residual interaction coupling constants κ_1^{01} and κ_1^0 . For $L > 0$ we have used the relations

$$\kappa_1^{LJ} = \frac{\kappa_1^{01}}{\langle r^{2L} \rangle} \quad \text{for the interaction (17)} \quad (31)$$

and

$$\kappa_1^{LJ} = \kappa_1^{01} \quad \text{for the interaction (18)} \quad (32)$$

In our theoretical total OMC rates final states with $J^\pi = 0^\pm, 1^\pm, 2^\pm$ and 3^\pm have been taken into account. Contributions from final states with $J > 3$ turned out to be less than 1%. In Table 3 and Fig. 1 we present the calculated total OMC rates for ^{90}Zr . The rates shown in Fig. 1 were calculated with both types of interaction, using $\kappa_1^0 = -0.43/A$ and $\kappa_1^{01} = -0.33/A$ for type (18) and $\kappa_1^0 = -35/A$ and $\kappa_1^{01} = -23/A$ for type (17). It can be seen that the main difference between the rates for the two different residual interactions originates from muon capture populating highly excited states. This difference is biggest for the 1^+ final states. Both calculated total rates agree with each other to within less than 5%. However, larger differences appear in the partial rates feeding states with a specific J^π . In general, one observes that for $A \approx 90$ nuclei the total capture rates calculated with the interaction (17) is larger than that calculated with the interaction (18).

The experimental total capture rate of $\Lambda = 86.6 \cdot 10^5 \text{ s}^{-1}$ [4] is in rather good agreement with both theoretical values. However, one should keep in mind that the experiment has been done with the natural isotope composition of ^{90}Zr , whereas the calculations refer to a specific isotope.

The theoretical capture rates Λ_{tot} show only a very slight sensitivity to a variation of g_p/g_n . The variation in Λ_{tot} for ^{90}Zr amounts to $85.5 \cdot 10^5 \text{ s}^{-1}$ to $76.8 \cdot 10^5 \text{ s}^{-1}$ if

g_p/g_A is increased from 4.0 to 12.0. The contribution of the velocity dependent matrix elements $[1wup]$ and $[0uup]$ to Λ_{tot} is rather small. The change in Λ_{tot} is less than 2% when they are switched off. The estimated contribution of (12 - 15)% made in [11] could thus not be confirmed by the direct calculation.

The interesting observation was made that the 1^+ state around 5 MeV which gives a prominent contribution in the $^{90}\text{Zr}(n,p)^{90}\text{Y}$ reaction, contributes only very little to the total muon capture rate. This is pointing to the fact that one cannot directly use matrix elements from (n,p) or (p,n) reactions to analyze muon capture data. A large B(GT) does not always imply a large capture rate Λ_{fi} . Here the explanation is that the radial matrix elements with spherical Bessel function $j_0(k_\nu r)$, dominating in allowed $0^+ \rightarrow 1^+$ partial transitions, are suppressed by the centrifugal barrier of the two-quasi particle state $(0g_{7/2})_n(0g_{9/2})_p$. This different appearance of the 1^+ state of the product nucleus in various reactions finds its explanation only within a microscopic nuclear model.

Table 4 and Table 5 contain the results of our calculation for ^{92}Mo . There is a satisfactory agreement between the experimental data and the rates obtained with our microscopic model. As in the case of ^{90}Zr the two different residual interactions lead to a different population of the specific J^π states which after summing over all final states is smoothed out. A comparison with the measured capture rate on natural Mo seems reasonable, since ^{92}Mo is the lightest even Mo-isotope, and the capture rate decreases with increasing neutron excess.

4.2 OMC on Even Tin Isotopes

In this section we consider the even tin isotopes $^{116-124}\text{Sn}$, a long chain of stable spherical nuclei. Tin isotopes have a completely filled $0g_{9/2}$ proton subshell and gradually filled $0g_{7/2}$, $1d_{5/2}$, $1d_{3/2}$ and $2s_{1/2}$ neutron subshells. Table 6 shows the total OMC rates calculated with two sets of single-particle potential parameters [17]. It can be seen that the dependence of the total capture rates on the Woods-Saxon potential parameters is stronger than its dependence on the residual interaction coupling constants. The calculated rates show also a strong dependence on the neutron excess of the target nucleus.

The experimental value of the capture rate measured for natural Sn is $106.7 \cdot 10^5 \text{ s}^{-1}$ [4]. Considering that $^{118,120}\text{Sn}$ contributes more than 50% to the natural isotope mixture, shows that the Woods-Saxon model parameters fitted to $A = 121, Z = 51$ give a better description of the total rates. We can say that the agreement between the theoretical capture rates and the experiment is quite good.

4.3 Heavy Nuclei with Large Neutron Excess. ^{140}Ce and ^{208}Pb

The most important observation to be made in the case of heavier nuclei is (see Fig. 2) the large theoretical overestimation of the rates. The difference between the calculated total OMC rates becomes larger with increasing mass number. Table 7 shows the results for ^{140}Ce and Table 8 those for ^{208}Pb . The rates calculated with the residual interaction (17) are smaller than those obtained with the interaction (18). This difference comes about mainly due to capture populating the high-excited 1^+ states which is absent in calculations using the interaction (17). The experimental energies of the collective IAS and GT (σt^-) states can be reproduced with the interaction (17) using $\kappa_1^0 = -28.0/A$ to obtain 18.94 MeV for the IAS state and using $\kappa_1^{01} = -23.0/A$ to obtain the GT state at an energy of 19.71 MeV. The corresponding experimental energies are 18.8 MeV for the IAS state and 19.2 MeV for the GT state respectively. More than 80% of the total GT strength sits at the peak of the distribution. Using the interaction (18) one obtains the collective 1^+ state at 16.85 MeV using $\kappa_1^{01} = -0.43/A$. Approximately 50% of the total GT strength goes to this state and more than 30% of the strength is shifted to the higher 1^+ states. These 1^+ states with high excitation energies are responsible for the fact that the collective 1^+ state remains in a region below 18 MeV even if $|\kappa_1^{01}|$ is doubled.

The experimental value of Λ_{tot} for ^{208}Pb is $135 \cdot 10^5 \text{ s}^{-1}$ [4]. Thus both calculations overestimate the total rate considerably. It is therefore interesting to compare our results with those from previous work achieving a good agreement with experiment [9, 11]. There is, however, a difficulty in performing this comparison because the authors of [9, 10, 11] presented their results as relative contributions to Λ_{tot} , related to a specific angular momentum transfer L . To compare these data to our results, we have to assume that the transitions to the 0^+ and 1^+ final states proceed via the $L = 0$ transition. The transitions to the $0^-, 1^-, 2^-$ states are accompanied by a $L = 1$ orbital angular momentum, etc. With this assumption we implicitly assume that $||[1J - 1J]|| \gg ||[1J + 1J]||$. A test shows that deleting of $[1J + 1J]$ reduces the corresponding Λ_{fi} by less than 10%. The fractional contributions obtained by this procedure are given in Table 9. A comparison with the results of [9, 10, 11] shows that the main difference to our results comes from the contributions of the $0^+ \rightarrow 1^+$ transition. This prominent role of the $0^+ \rightarrow 1^+$ transition was also found in a recent calculation [12]. The total OMC rate for ^{208}Pb obtained in the present work with the interaction (17) compares well with the value $\Lambda_{tot}(^{208}\text{Pb}) = 161 \cdot 10^5 \text{ s}^{-1}$ obtained in [12] using a δ -function residual interaction.

5 Discussion and Conclusion

In this work a theoretical evaluation of the total OMC rates for medium - weight and heavy spherical nuclei using QRPA was presented. For the first time an attempt was made to include the velocity-dependent terms, evaluated with single particle wave functions having the correct asymptotic behaviour. It was shown that the contribution of these terms to $\Lambda_{\text{tot}}^{\text{theor}}$ is rather small. To avoid confusion, some remarks about the meaning of "velocity-dependent" terms have to be made. Usually all terms having its origin in the small components of the nucleon 4-spinors are called "velocity-dependent" terms. However, in the derivation of the effective muon capture Hamiltonian [15], part of these terms experience a transformation due to momentum conservation

$$\vec{p} + \vec{\mu} = \vec{n} + \vec{\nu}, \quad |\vec{\mu}| \approx 0, \quad \Rightarrow \quad \vec{n} = \vec{p} - \vec{\nu}. \quad (33)$$

As a result, only the gradient acting on the proton wave functions is left. We have explicitly shown that the matrix elements with the proton gradient give a minor contribution to the capture rate. So one can conclude that the main effect of the velocity-dependent terms is already accounted for in the effective Hamiltonian due to momentum conservation.

Our calculations show that the total OMC rates are not very sensitive to the constants of the nuclear residual interactions. On the other hand they may strongly depend on the shape of the residual interaction used in the calculations. The main influence on Λ_{tot} calculated with different residual interactions comes from the difference in the description of GT transitions, $0^+ \rightarrow 1^+$, especially at higher excitation energies.

A comparison of our theoretical total OMC rates with experiments shows (Table 10 and Fig. 2) the following situation. For the medium weight nuclei (^{90}Zr , $^{116-124}\text{Sn}$) a reasonable agreement between theory and experiment can be achieved using the free values of g_A and g_P . No renormalization of g_A is needed in this mass region.

The $\Lambda_{\text{tot}}^{\text{theor}}$ exceed, however, considerably the experimental values for the heavier nuclei ^{140}Ce and ^{208}Pb . Therefore, in order to reproduce the experimental values, a renormalization of g_A seems to be necessary for heavy nuclei. This renormalization is model dependent; it depends in our case on the coupling constants and the shape of the residual interaction, as can be seen from Table 7 and 8. From Fig. 2 one is tempted to deduce some systematic deviation of $\Lambda_{\text{tot}}^{\text{theor}}$ from the experimental data. This makes it impossible to draw any definite conclusion on the necessity of a quenching of g_A for heavier nuclei. It seems that the nuclear model used in this investigation reaches its limits of useful application so that further theoretical studies are necessary. The widespread belief [11] that a theoretical description of total OMC rates faces no particular problem seems to be untenable.

Acknowledgements

We would like to thank R. Rosenfelder for many helpful discussions and improvements while reading the text. Two of us, V. A. Kuzmin and T. V. Tetereva, would like to express their gratitude for the support obtained from PSI which made several visits to this institute possible.

References

- [1] I.S. Towner, J.C. Hardy, in *The Nucleus as a Laboratory for Studying Symmetries and Fundamental Interactions*, Eds. E.M. Henley, W.C. Haxton; Singapore, New Jersey, London, Hong Kong: World Scientific Publ. Co. Pte. Ltd., 1995, p. 183.
- [2] M. Gmitro, A.A. Ovchinnikova, T.V. Tetereva, *Nucl. Phys. A* **453**(1986), 685.
- [3] R.A. Eramzhyan, V.A. Kuz'min, and T.V. Tetereva, *Nucl. Phys. A* **642**(1998), 428.
- [4] T. Suzuki, D.F. Measday, J.P. Roalsvig, *Phys. Rev. C* **35**(1987), 2212.
- [5] B. Goulard, H. Primakoff, *Phys. Rev. C* **10**(1974), 2034.
- [6] J. Navarro, J. Bernabeu, J.M. Gomez, J. Martorell, *Nucl. Phys. A* **375**(1987), 361.
- [7] H.C. Chiang, E. Oset, P. Fernandez de Cordoba, *Nucl. Phys. A* **510**(1990), 591.
- [8] H.W. Fearing, M.S. Welsh, *Phys. Rev. C* **46**(1992), 2077.
- [9] G.G. Bunatian, *Sov. J. Nucl. Phys.* **3**(1966), 613.
- [10] N. Auerbach, L. Zamick, A. Klein, *Phys. Lett. B* **118**(1982), 256;
N. Auerbach, A. Klein, *Nucl. Phys. A* **422**(1984), 480.
- [11] M.G. Urin, and O.N. Vyazankin, *Nucl. Phys. A* **537**(1992), 534.
- [12] E. Kolbe, K. Langanke, P. Vogel, preprint nucl-th/0006007 (2000).
- [13] M. Morita, and A. Fujii, *Phys. Rev.* **118**(1960), 606.
- [14] G.E. Pustovalov, *Sov. Phys. JETP.* **36(9)**(1959), 1288.
- [15] V.V. Balashov, G.Ya. Korenman, and R.A. Eramzhyan,
“Poglozhenie mezonov atomnymi yadrami”, M., 1978 (in Russian).
- [16] V. G. Soloviev, *Theory of Complex Nuclei*, Oxford, Pergamon, 1976.
- [17] V.Yu. Ponomarev, *et al*, *Nucl. Phys. A* **323**(1979), 446.
- [18] A.I. Vdovin, and V.G. Soloviev, *Sov. J. Part. Nucl.* **14**(1983), 237.
- [19] D.E. Bainum, *et al.*,
Phys. Rev. Lett. **44**(1980), 1751.

- [20] T. Wakasa, H. Sakai, H. Okamura, *et al.* Phys. Rev. **C 55**(1997), 2909.
- [21] M. Moosburger, E. Aschenauer, H. Dennert, *et al.* Phys. Rev. **C 57**(1998), 602.
- [22] K. Ikeda, S. Fujii, and J.I. Fujita, Phys. Lett. **63**(1963), 271.
- [23] C. Gaarde, *et al.*, Nucl. Phys. **A 369**(1981), 258.
- [24] V.A. Kuz'min, Phys. Atom. Nucl. **58**(1995), 368;
K. Junker, V.A. Kuz'min, T.V. Tetereva, Eur. Phys. J. **A 5**(1999), 37.
- [25] K.J. Raywood, *et al.*, Phys. Rev. **C 41**(1990), 2836.
- [26] W.J. Courtney, and J.D. Fox, At. Data and Nucl. Data Tabl. **15**(1975), 141.

Table 1: Properties of charge-exchange 1^+ excitations in ^{90}Zr calculated with two variants of residual interactions.

$\kappa_1^{01}A$	σt^- as in (p, n) reaction				σt^+ as in (n, p) reaction			
	Energy of maximum	$B^-(GT)$			Energy of maximum	$B^+(GT)$		
		total	in max.	below max.		total	in max.	below max.
0.00	11.84	32.06	16.96	13.79	5.34	3.32	2.21	0.00
				$f(r) = dU/dr$				
-0.23	14.93	31.89	20.88	6.23	5.62	3.15	1.31	0.00
-0.33	15.76	32.03	19.88	4.67	5.68	3.30	1.14	0.00
-0.43	16.36	32.21	18.41	3.74	5.73	3.47	1.03	0.00
				$f_L(r) = r^L$				
-23.0	15.73	30.63	23.83	5.32	5.63	1.89	1.12	0.00
-25.0	16.09	30.56	23.98	4.86	5.65	1.82	1.07	0.00
-28.0	16.63	30.05	23.86	4.28	5.67	1.72	0.99	0.00

Table 2: Properties of charge-exchange 0^+ excitations in ^{90}Zr calculated with two variants of residual interactions.

$\kappa_1^0 A$	t^-				t^+			
	Energy of maximum	B^-			Energy of maximum	B^+		
		total	in max.	below max.		total	in max.	below max.
0.00	4.62	10.14	8.62	0.00	16.17	0.29	0.07	0.13
				$f(r) = dU/dr$				
-0.33	10.99	10.58	8.30	0.37	18.08	0.72	0.55	0.16
-0.43	12.00	10.70	7.94	0.14	18.34	0.84	0.67	0.16
-0.53	12.81	10.81	7.44	0.07	18.56	0.96	0.79	0.15
				$f_L(r) = r^L$				
-23.00	10.35	10.04	7.87	1.78	16.91	0.18	0.05	0.07
					16.20		0.04	
-25.00	10.71	10.03	8.29	1.32	16.92	0.18	0.05	0.07
					16.20		0.04	
-28.00	11.28	10.02	8.68	0.88	16.92	0.17	0.05	0.07
					16.20		0.04	
-31.00	11.87	10.02	8.88	0.62	16.92	0.16	0.05	0.06
					16.20		0.04	
-34.00	12.46	10.01	8.96	0.45	16.93	0.15	0.05	0.06
					16.20		0.04	
-37.00	13.06	10.00	8.97	0.34	16.93	0.15	0.04	0.05
					16.21		0.03	

Table 3: The rates of OMC (in 10^5 s^{-1}) on ^{90}Zr summed over the final states with specific spin and parity J^π . The second line gives the contribution of each final state in %.

κ_1^{LJA}	final states, J^π								total rate
	0^+	0^-	1^+	1^-	2^+	2^-	3^+	3^-	
0.00	4.9	3.6	24.3	43.4	15.2	19.3	11.6	3.3	125.6
	3.9	2.8	19.3	34.6	12.1	15.4	9.2	2.6	100.0%
$f(r) = dU/dr$									
-0.23	5.3	2.2	28.3	27.3	8.5	12.3	5.5	1.4	90.8
	5.9	2.5	31.2	30.0	9.3	13.5	6.0	1.6	100.0%
-0.33	5.3	2.2	29.1	25.1	7.4	11.2	4.4	1.2	85.8
	6.2	2.5	33.9	29.2	8.6	13.1	5.2	1.4	100.0%
-0.43	5.3	2.2	29.9	23.5	6.6	10.5	3.7	1.0	82.8
	6.4	2.6	36.1	28.4	8.0	12.7	4.5	1.2	100.0%
$f_L(r) = r^L$									
-23.0	4.7	1.9	23.4	27.2	10.2	12.2	7.1	1.9	88.7
	5.3	2.2	26.4	30.6	11.5	13.8	8.0	2.2	100.0%
-25.0	4.7	1.9	23.2	27.2	10.0	11.8	6.9	1.9	86.9
	5.5	2.2	26.7	26.5	11.5	13.6	7.9	2.2	100.0%
-28.0	4.7	1.8	23.0	25.7	9.6	11.3	6.5	1.8	84.4
	5.6	2.1	27.2	30.4	11.4	13.4	7.8	2.1	100.0%

Table 4: Properties of charge-exchange 1^+ excitations in ^{92}Mo calculated with two different nuclear residual interactions.

$\kappa_1^{01}A$	σt^- as in (p, n) reaction				σt^+ as in (n, p) reaction			
	Energy of maximum	$B^-(GT)$			Energy of maximum	$B^+(GT)$		
		total	in max.	below max.		total	in max.	below max.
0.00	11.85	28.79	16.94	10.70	4.44	5.96	4.75	0.00
				$f(r) = dU/dr$				
-0.23	14.98	27.42	11.61	12.17	5.04	4.59	2.92	0.00
-0.33	15.61	27.28	16.94	4.83	5.19	4.45	2.57	0.00
-0.43	16.15	27.23	16.50	3.42	5.29	4.40	2.33	0.00
				$f_L(r) = r^L$				
-23.0	15.54	26.36	18.36	6.86	5.07	3.53	2.56	0.00
-25.0	15.81	26.23	19.40	5.61	5.11	3.40	2.45	0.00
-28.0	16.25	26.06	20.20	4.47	5.16	2.23	2.29	0.00

Table 5: The rates of OMC (in 10^5 s^{-1}) on ^{92}Mo summed over the final states with specific spin and parity J^π . The second line gives the contribution of each final state in %.

κ_1^{LJA}	final state J^π								total rate
	0 ⁺	0 ⁻	1 ⁺	1 ⁻	2 ⁺	2 ⁻	3 ⁺	3 ⁻	
0.00	5.3	4.1	27.4	52.2	18.1	24.2	13.5	3.8	148.7
	3.6	2.8	18.4	35.1	12.2	16.3	9.1	2.6	100.0%
$f(r) = dU/dr$									
-0.23	5.6	2.5	30.5	33.3	10.1	15.6	6.5	1.7	105.8
	5.3	2.4	28.8	31.5	9.5	14.7	6.2	1.6	100.0%
-0.33	5.6	2.4	31.0	30.6	8.8	14.1	5.3	1.4	99.2
	5.6	2.4	31.3	30.8	8.8	14.2	5.4	1.4	100.0%
-0.43	5.6	2.4	31.5	28.7	7.8	13.2	4.5	1.2	95.0
	5.9	2.6	33.2	30.3	8.3	13.9	4.8	1.8	100.0%
$f_L(r) = r^L$									
-23.0	5.1	2.3	26.2	33.6	12.3	15.9	8.5	2.3	106.2
	4.8	2.1	24.6	31.6	11.6	15.0	8.0	2.1	100.0%
-25.0	5.1	2.2	26.0	32.9	12.0	15.5	8.2	2.2	104.1
	4.9	2.1	24.9	31.6	11.5	14.9	7.9	2.2	100.0%
-28.0	5.1	2.1	25.7	31.8	11.6	14.9	7.9	2.2	101.2
	5.1	2.1	25.4	31.5	11.5	14.7	7.8	2.1	100.0%

Table 6: Total OMC capture rates on Sn isotopes (in 10^5 s^{-1}).

Target nucleus	$\kappa_1^{01} A$ for (18)	SW parameters		$\kappa_1^{01} A$ for (17)	SW parameters	
		115,49	121,51		115,49	121,51
^{116}Sn	-0.23	139.2	130.1	-23.0	141.7	123.0
	-0.33	130.5	123.1	-25.0	138.9	120.8
	-0.43	124.9	119.0	-28.0	135.2	117.4
^{118}Sn	-0.23	130.0	122.1	-23.0	131.9	115.0
	-0.33	122.1	116.1	-25.0	129.4	112.7
	-0.43	117.1	112.4	-28.0	125.9	109.5
^{120}Sn	-0.23	121.2	111.8	-23.0	122.6	107.3
	-0.33	114.2	109.5	-25.0	120.3	104.1
	-0.43	109.8	106.3	-28.0	117.2	102.1
^{122}Sn	-0.23	113.2	107.8	-23.0	114.0	99.7
	-0.33	106.9	103.2	-25.0	118.0	97.7
	-0.43	103.0	100.6	-28.0	108.0	95.0
^{124}Sn	-0.23	105.5	101.3	-23.0	105.5	91.7
	-0.33	99.9	97.1	-25.0	103.4	89.9
	-0.43	96.5	95.1	-28.0	100.7	88.3

Table 7: The rates of OMC (in 10^5 s^{-1}) on ^{140}Ce summed over final states with specific spin and parity J^π . The second line gives the contribution of each final state in %.

κ_1^{LJA}	final state J^π								total rate
	0^+	0^-	1^+	1^-	2^+	2^-	3^+	3^-	
$f(r) = dU/dr$									
-0.23	11.7	3.8	55.4	39.9	20.2	21.0	10.3	3.5	165.7
	7.0	2.3	33.4	24.1	12.2	12.7	6.2	2.1	100.0%
-0.33	11.7	3.5	57.4	38.0	17.9	21.3	8.7	2.9	161.2
	7.2	2.2	35.6	23.5	11.1	13.2	5.4	1.8	100.0%
-0.43	11.7	3.4	59.2	36.7	16.2	21.7	7.7	2.5	159.0
	7.3	2.1	37.3	23.1	10.2	13.7	4.8	1.6	100.0%
$f_L(r) = r^L$									
-23.0	9.8	3.4	41.4	35.8	25.2	15.1	12.9	5.1	148.9
	6.6	2.3	27.8	24.1	16.9	10.1	8.7	3.4	100.0%
-25.0	9.8	3.3	41.2	35.1	24.7	14.8	12.5	5.0	146.3
	6.7	2.2	28.1	24.0	16.9	10.1	8.6	3.4	100.0%
-28.0	9.8	3.1	40.8	34.1	23.9	14.4	12.0	4.8	142.8
	6.9	2.2	28.5	23.9	16.7	10.1	8.4	3.4	100.0%

Table 8: The rates of OMC (in 10^5 s^{-1}) on ^{208}Pb summed over final states with specific spin and parity J^π . The second line gives the contribution of each final state in %.

κ_1^{LJA}	final state J^π								total rate
	0^+	0^-	1^+	1^-	2^+	2^-	3^+	3^-	
$f(r) = dU/dr$									
-0.23	15.7	3.1	70.5	33.8	29.7	29.5	10.4	5.8	198.6
	7.9	1.6	35.5	17.0	15.0	14.9	5.2	2.9	100.0%
-0.33	15.7	2.7	72.5	33.1	26.9	31.8	9.5	4.9	197.2
	8.0	1.4	36.8	16.8	13.7	16.1	4.8	2.5	100.0%
-0.43	15.7	2.4	71.9	32.6	25.0	33.2	9.0	4.3	194.2
	8.1	1.2	37.0	16.8	12.9	17.1	4.6	2.2	100.0%
$f_L(r) = r^L$									
-23.0	13.5	2.8	46.9	23.8	33.7	19.9	11.0	8.0	159.5
	8.5	1.7	29.4	14.9	21.1	12.4	6.9	5.0	100.0%
-25.0	13.5	2.6	46.7	23.3	33.0	19.8	10.7	7.8	157.4
	8.6	1.7	29.7	14.8	21.0	12.6	6.8	5.0	100.0%
-28.0	13.5	2.4	46.5	22.6	32.0	19.6	10.3	7.5	154.5
	8.7	1.6	30.1	14.7	20.7	12.7	6.7	4.9	100.0%

Table 9: Fractional contributions of different multipoles to Λ_{tot} for ^{208}Pb (either contributions of the orbital momentum transfer or contributions of the transitions to the states with specific J^π).

Reference	ΔL							
	0	1	2	3				
[9]	26	14	48	12				
[10]	29	13	52	7				
[11]	23	34	34	8				
(a)	$\simeq 45$	$\simeq 35$	$\simeq 18$	$\simeq 2$				
(b)	$\simeq 38$	$\simeq 29$	$\simeq 27$	$\simeq 5$				
	J^π							
	0^+	1^+	0^-	1^-	2^-	2^+	3^+	3^-
[12]	5	36	6	14	12	28	4	2
(a)	8	37	2	17	16	14	5	3
(b)	8	30	2	15	12	21	7	5

- (a) – present paper, calculations with the residual interaction (18), $\kappa_1^{LJ} \cdot A = -0.43$;
(b) – present paper, calculations with the residual interaction (17), $\kappa_1^{LJ} \cdot A = -25.0$.

Table 10: Summary of results : total OMC rates (in 10^5 s^{-1}) calculated for $g_P/g_A = 6.0$ with two different radial form factors of the nuclear residual interaction.

Target nucleus	$\kappa_1^{LJ} A$ for dU/dr			$\kappa_1^{LJ} A$ for r^L			expr. [4]
	-0.23	-0.33	-0.43	-23.0	-25.0	-28.0	
^{90}Zr	90.8	85.8	82.8	88.7	86.8	84.4	86.6
^{92}Mo	105.8	99.2	95.0	106.2	104.1	101.2	92.2
^{116}Sn	130.1	123.2	119.0	123.2	120.8	117.4	
^{118}Sn	122.1	116.1	112.4	115.0	112.7	109.5	
^{120}Sn	114.8	109.5	106.3	107.3	105.1	102.1	106.7
^{122}Sn	107.8	103.2	100.6	99.7	97.7	95.0	
^{124}Sn	101.3	97.1	95.1	91.7	89.9	88.3	
^{140}Ce	165.7	161.2	159.0	148.9	146.3	142.8	114.4
^{208}Pb	198.6	197.2	194.2	159.5	157.4	154.5	134.5

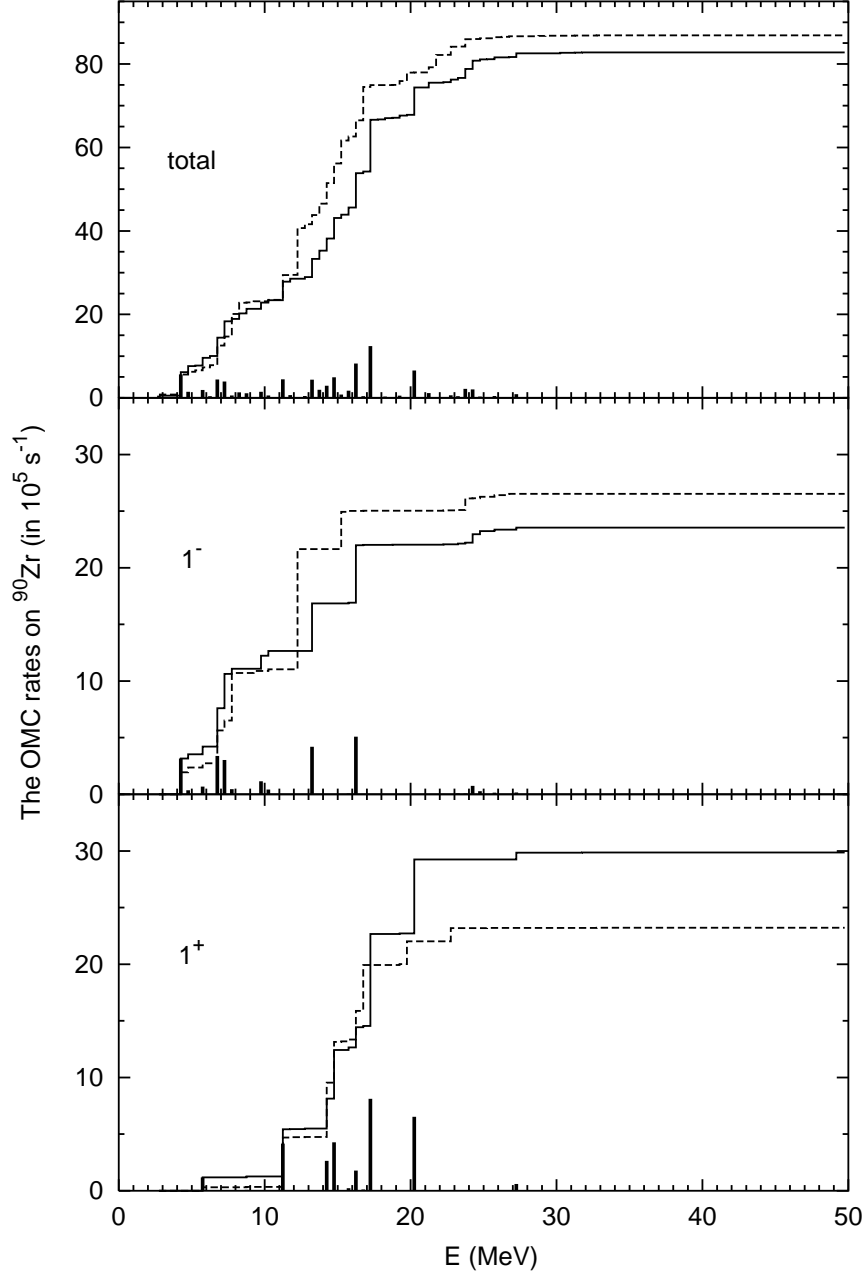


Figure 1: ^{90}Zr : Total and partial integrated capture rates up to the excitation energy E of the final nucleus. The partial rates are shown for the final states with $J^\pi = 1^\pm$. Solid lines: results of the calculation with the residual interaction (18), dashed lines: the same with the interaction (17), the solid vertical bars show the distribution of the calculated partial rates over the excited states with $J^\pi = 1^\pm$. In the upper part of the figure the distribution over all excited states is shown.

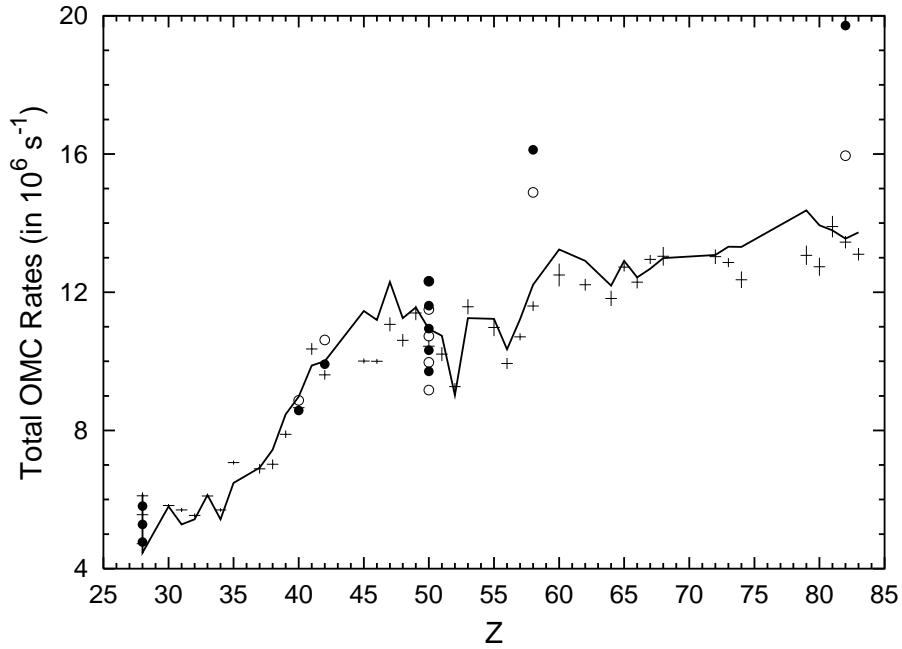


Figure 2: Comparison between experimental and calculated total capture rates. Crosses: experimental data taken from [3] and [4] (the vertical extension indicates the experimental error), full circles: calculation with the interaction (18), open circles: calculation with the interaction (17). The full curve connects the rates calculated with the Goulard - Primakoff formula [5] with its parameters determined from [4].

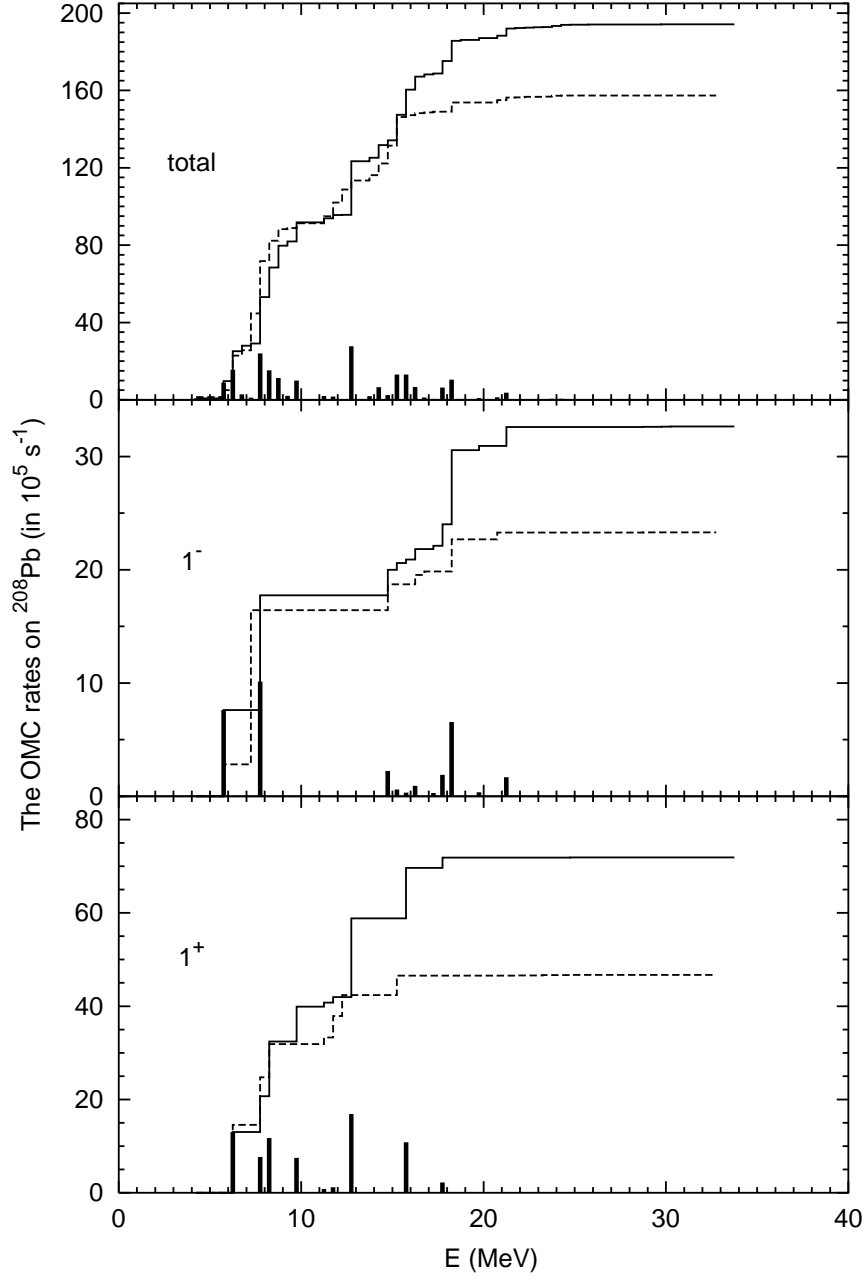


Figure 3: ^{208}Pb : Total and partial integrated capture rates up to the excitation energy E of the final nucleus. The partial rates are shown for the final states with $J^\pi = 1^\pm$. Solid lines: results of the calculation with the residual interaction (18), dashed lines: the same with the interaction (17), the solid vertical bars show the distribution of the calculated partial rates over the excited states with $J^\pi = 1^\pm$. In the upper part of the figure the distribution over all excited states is shown.